Tran-SET

A Deep Learning Tool for the Assessment of Pavement Smoothness and Aggregate Segregation during Construction

Project No. 21COLSU14

Lead University: Louisiana State University

Final Report

March 2023

Disclaimer

Acknowledgements

1. TECHNICAL DOCUMENTATION PAGE

1. Project No.	2. Government Accession No.	3. Recipient's Catalog No.	
21COLSU14			
4. Title and Subtitle A Deep Learning Tool for the Assessment of Pavement Smoothness and Aggregate Segregation during Construction		**5. Report Date** Aug. 2022	
		6. Performing Organization Code	
7. Author(s) Mostafa A Elseifi, Ramchandra Paudel, Md Tanvir Ahmed Sarkar, Hossam Abohamer, and Nirmal Dhakal		**8. Performing Organization Report No.**	
9. Performing Organization Name and Address Transportation Consortium of South-Central States (Tran-SET)		**10. Work Unit No. (TRAIS)**	
University Transportation Center for Region 6 3319 Patrick F. Taylor Hall, Louisiana State University, Baton Rouge, LA 70803		**11. Contract or Grant No.** 69A3551747106	
12. Sponsoring Agency Name and Address United States of America Department of Transportation Research and Innovative Technology Administration		**13. Type of Report and Period Covered** Final Research Report Mar. 2018 – Mar. 2019	
		14. Sponsoring Agency Code	

15. Supplementary Notes

Report uploaded and accessible at Tran-SET's website (http://transet.lsu.edu/).

16. Abstract

Pavement construction monitoring and quality assurance (QA) practices are mostly based on costly, discrete, and destructive methods. Most quality assurance programs are based on pavement construction procedures encompassing in-situ coring for layer thickness determination, density measurements, laboratory testing to measure volumetric properties, and smoothness measurements in case of the availability of a profiler. The main objective of this study was to develop a machine learning-based classifier for predicting pavement roughness and aggregate segregation based on digital image analysis, image recognition, and deep learning machine models. The developed Convolution Neural Networks (CNN) models were trained, tested, and validated using 600-pavement surface images extracted from the Louisiana Department of Transportation and Development (LaDOTD) Pavement Management System (PMS) and 129 pavement images collected from three construction sites a few days after paving. These images were randomly divided into 70%, 15%, and 15% for the training, testing, and validation phases, respectively. The roughness model achieved 93.8% and 92.6% accuracy in the training and validation stages; respectively, and predicted the International Roughness Index (IRI) values with a coefficient of determination R^2 of 0.98 and a Root-Mean Square Error (RMSE) of 3.5%. In addition, the developed image-processing model for the detection of aggregate segregation achieved adequate accuracy. Furthermore, the developed segregation detection procedure adequately described the relationship between mix density and segregation.

| **17. Key Words**
 Pavement, Roughness, Segregation, Road Construction, Quality Assurance | | **18. Distribution Statement**
 No restrictions. This document is available through the National Technical Information Service, Springfield, VA 22161. | |
| **19. Security Classif. (of this report)**
 Unclassified | **20. Security Classif. (of this page)**
 Unclassified | **21. No. of Pages**
 38 | **22. Price** |

Form DOT F 1700.7 (8-72)   **Reproduction of completed page authorized.**

SI* (MODERN METRIC) CONVERSION FACTORS

APPROXIMATE CONVERSIONS TO SI UNITS

Symbol	When You Know	Multiply By	To Find	Symbol
LENGTH				
in	inches	25.4	millimeters	mm
ft	feet	0.305	meters	m
yd	yards	0.914	meters	m
mi	miles	1.61	kilometers	km
AREA				
in^2	square inches	645.2	square millimeters	mm^2
ft^2	square feet	0.093	square meters	m^2
yd^2	square yard	0.836	square meters	m^2
ac	acres	0.405	hectares	ha
mi^2	square miles	2.59	square kilometers	km^2
VOLUME				
fl oz	fluid ounces	29.57	milliliters	mL
gal	gallons	3.785	liters	L
ft^3	cubic feet	0.028	cubic meters	m^3
yd^3	cubic yards	0.765	cubic meters	m^3
NOTE: volumes greater than 1000 L shall be shown in m^3				
MASS				
oz	ounces	28.35	grams	g
lb	pounds	0.454	kilograms	kg
T	short tons (2000 lb)	0.907	megagrams (or "metric ton")	Mg (or "t")
TEMPERATURE (exact degrees)				
^oF	Fahrenheit	5 (F-32)/9 or (F-32)/1.8	Celsius	^oC
ILLUMINATION				
fc	foot-candles	10.76	lux	lx
fl	foot-Lamberts	3.426	candela/m^2	cd/m^2
FORCE and PRESSURE or STRESS				
lbf	poundforce	4.45	newtons	N
lbf/in^2	poundforce per square inch	6.89	kilopascals	kPa

APPROXIMATE CONVERSIONS FROM SI UNITS

Symbol	When You Know	Multiply By	To Find	Symbol
LENGTH				
mm	millimeters	0.039	inches	in
m	meters	3.28	feet	ft
m	meters	1.09	yards	yd
km	kilometers	0.621	miles	mi
AREA				
mm^2	square millimeters	0.0016	square inches	in^2
m^2	square meters	10.764	square feet	ft^2
m^2	square meters	1.195	square yards	yd^2
ha	hectares	2.47	acres	ac
km^2	square kilometers	0.386	square miles	mi^2
VOLUME				
mL	milliliters	0.034	fluid ounces	fl oz
L	liters	0.264	gallons	gal
m^3	cubic meters	35.314	cubic feet	ft^3
m^3	cubic meters	1.307	cubic yards	yd^3
MASS				
g	grams	0.035	ounces	oz
kg	kilograms	2.202	pounds	lb
Mg (or "t")	megagrams (or "metric ton")	1.103	short tons (2000 lb)	T
TEMPERATURE (exact degrees)				
^oC	Celsius	1.8C+32	Fahrenheit	^oF
ILLUMINATION				
lx	lux	0.0929	foot-candles	fc
cd/m^2	candela/m^2	0.2919	foot-Lamberts	fl
FORCE and PRESSURE or STRESS				
N	newtons	0.225	poundforce	lbf
kPa	kilopascals	0.145	poundforce per square inch	lbf/in^2

2. TABLE OF CONTENTS

3. LIST OF FIGURES

4. LIST OF TABLES

5. ACRONYMS, ABBREVIATIONS, AND SYMBOLS

Term	Description
AC	Asphalt Concrete
AASHTO	American Association of State Highway and Transportation Officials
AI	Artificial Intelligence
ANN	Artificial Neural Networks
ANOVA	Analysis of Variance
ARAN	Automatic Road Analyzer
ASTM	American Society for Testing and Materials
BEMD	Bidimensional Empirical Mode Decomposition
CNN	Convolution Neural Networks
DCNN	Deep Convolutional Neural Networks
DL	Deep Learning
ESALs	Equivalent Single Axle Loads
HMA	Hot-Mix Asphalt
IRI	International Roughness Index
LaDOTD	Louisiana Department of Transportation and Development
NDT	Non-Destructive Testing
PMS	Pavement Management System
PSPA	Portable Seismic Pavement Analyzer
QA	Quality Assurance
RBM	Restricted Boltzman Machines

6. EXECUTIVE SUMMARY

Most state QA programs are based on pavement construction procedures that encompass in-situ coring for layer thickness determination, density measurements, and laboratory testing to measure volumetric properties. In general, these methods are slow, costly, and time-consuming. Research studies indicate that Non-Destructive Testing (NDT) methods have the potential for use in the Quality Assurance (QA) of pavement construction since they allow for (a) fast evaluation of the product uniformity in real time as construction progresses; (b) identifying potential defects during construction to allow for timely corrective actions; (c) more frequent inspecting, testing, and replicating without the damaging effects of coring and other destructive testing; and (d) reducing the testing and inspections costs, while improving construction quality.

The use of pavement smoothness in QA programs has increased significantly in recent years. Pavement smoothness is measured using a profilometer or a laser-based surface tester, also known as an inertial profiler. Including surface profile smoothness tolerance requirements in specifications also allows for an additional payment incentive (bonus) or penalty based on the contractor's performance. While the use of smoothness specifications is a positive development in QA programs to assess construction quality, the availability of a profiler in most of the road construction projects is a major obstacle for widespread implementation of this practice. Hence, the measurement of pavement smoothness and the detection of aggregate segregation in real-time or upon completion of the construction process is limited by the availability of an inertial profiler. This may result in inadequate construction quality, early pavement failure, poor ride quality, and the inability to introduce timely remedies to address the noted deficiencies.

The objective of this study was to develop and validate machine learning models based on Convolutional Neural Networks (CNN) and digital image analysis that can be used to classify pavement surface into different IRI categories, to predict IRI values, and to detect the presence of aggregate segregation on the pavement surface of a newly-constructed road section. To achieve this objective, two CNN models were developed based on the ResNet Architecture; one model predicted the roughness categories (Good or Very Good) from the feature analysis of the pavement images. The second model predicted the roughness values using IRI from the feature analysis of the pavement images. These models were trained, tested, and validated using 600-pavement surface images extracted from the LaDOTD pavement management system and 129 pavement images collected from three construction sites. These images were randomly divided into 70%, 15%, and 15% for the training, testing, and validation phases, respectively. The images from the two data sources were used in the three phases to adapt the model to accurately respond to both types of pavement images.

For the development of the segregation model, a segregation parameter (S) was introduced to assess the relative distribution of particle aggregate sizes on a grid defined by 4,096 equally-distributed squares. The calculated S-value was then used to detect and quantify the presence of segregation on the pavement surface. A S-value of zero indicates no aggregate segregation, a positive value indicates a coarse aggregate segregation, while a negative value indicates a fine aggregate segregation. By categorizing the S-value for each square on a captured image, a colored map was generated based on the calculated S-values for the 4,096 squares. Multiple examples are presented to detect segregation based on this innovative approach.

Based on the results of the analysis, it was determined that the roughness classification model achieved an overall accuracy of 93.8% in the training phase and 92.6% in the validation phase. In

addition, the IRI prediction model had an acceptable accuracy with a coefficient of determination (R^2) of 0.99 and a root-mean-square error (RMSE) of 3.5%. Visual comparison between the digital images and the colored segregation maps showed good agreement. The developed segregation detection procedure adequately described the relationship between mix density and segregation by predicting an increase in S-value with the decrease in mix density.

Based on the results of this study, a computer application was developed for the AI models by creating a standalone tool, which would allow the site engineers to use the developed models without the need for coding software on their device. Future development of the application may allow the users to retrain the adaptive models to ensure up-to-date accuracy.

1. INTRODUCTION

1.1 Problem Statement

Research studies indicate that Non-Destructive Testing (NDT) methods have the potential for use in the Quality Assurance (QA) of pavement construction since they allow for (a) fast evaluation of the product uniformity in real time as construction progresses; (b) identifying potential defects during construction to allow for timely corrective actions; (c) more frequent inspecting, testing, and replicating without the damaging effects of coring and other destructive testing; and (d) reducing the testing and inspections costs, while improving construction quality. Results of NCHRP 10-65 recommended to use the GeoGauge for estimating the modulus of unbound layers and the portable seismic pavement analyzer (PSPA) for estimating the modulus of Hot Mix Asphalt (HMA) layers *(1)*. However, in spite of their high potential and usefulness, the transition of NDT methods from research to practice has been limited, and the destructive and time-consuming process of coring and laboratory testing continues to be the most widely used QA methods in the US.

The use of pavement smoothness in QA programs has increased significantly in recent years. Pavement roughness, which is the opposite of pavement smoothness, is described in terms of the International Roughness Index (IRI) and is a measure of ride quality and driver's comfort. IRI represents the deviation of the pavement surface from the leveled plan that affects vehicle movement and ride quality *(2)*. Pavement smoothness is measured using a profilometer or a laser-based surface tester, also known as an inertial profiler. Technically, IRI is the cumulative vertical displacement of an axle from a reference quarter-car divided by the distance traveled over the pavement profile at a standard speed of 50 mph. Many new specifications require all mainline paving meet surface profile smoothness tolerance using IRI for quality assurance requirements. Including surface profile smoothness tolerance requirements in specifications also allows for an additional payment incentive (bonus) or penalty based on the contractor's performance.

Figure 1. Aggregate Segregation and Non-Uniform Texture after Construction *(3)*

While the use of smoothness specifications is a positive development in QA programs to assess construction quality, the availability of a profiler in most of the road construction projects is a major obstacle for widespread implementation of this practice. Hence, the measurement of pavement smoothness and the detection of aggregate segregation in real-time or upon completion of the construction process is limited by the availability of an inertial profiler. This may result in inadequate construction quality, early pavement failure, poor ride quality, and the inability to introduce timely remedies to address the noted deficiencies.

1.2 Background

Until the early 2000s, the collection of pavement condition data and distress survey were mostly conducted using manual visual methods *(4)*. However, manual visual methods are slow, costly, and presents safety risk to the surveyor; these limitations led state agencies to adopt automated distress survey using devices such as Roadware's Automatic Road Analyzer (ARAN) system and Road Measurement Data Acquisition System (ROMAS), which allow to collect pavement condition data at traffic speed and without traffic disruption. In Louisiana, ARAN surveys are conducted every two years on in-service roads to collect pavement surface conditions. Yet, ARAN costs around $1.2 million and has an annual operating cost of $70,000. In these surveys, pavements are scanned with a vehicle equipped with cameras, lasers, sensors, and computers, to collect high-definition digital images of pavement surfaces, which are then used to assess in-service pavement conditions.

Concurrent with the introduction of automated distress surveys, researchers have developed computer vision and machine learning techniques to automate the process of pavement data collection and condition evaluation *(2)*. Most of these applications focused on detecting, classifying, and quantifying existing distresses including cracks, rutting, and roughness. However, the application of computer vision for the extraction of features such as pavement roughness has not been thoroughly investigated. Recently, Convolutional Neural Networks (CNN) have been successfully implemented in object recognition and image classification. In transportation, CNN have received considerable attention in pavement condition evaluation and crack detection and quantification *(5-6)*. CNN do not require extensive pre-processing steps; in addition, they can identify and differentiate many features such as cracks and potholes from the analyzed images.

While pavement condition evaluation has successfully transitioned to automated inspection and data collection, construction monitoring, and quality assurance practices are still based on costly and destructive methods. In addition, most state QA programs are based on pavement construction procedures that encompass in-situ coring for layer thickness determination, density measurements, laboratory testing to measure volumetric properties, and smoothness measurements in case of the availability of an inertial profiler. In general, these methods are slow, costly, and time-consuming. Furthermore, QA programs are based on empirical specifications that are principally designed to ensure that all the critical raw ingredients are used in the installed paving mat. This approach leads to poor construction quality, rough surfaces, segregated asphalt mixes, and premature pavement failure.

2. OBJECTIVES

The aim of this study was to develop non-destructive tools based on pavement surface image analysis and machine learning models; these tools can be used to assess the quality of asphalt paving construction by predicting surface roughness and by detecting aggregate segregation. To achieve this goal, the main objectives of this study were to develop and validate machine learning models based on Convolutional Neural Networks (CNN) and digital image analysis that can be used to classify pavement surface into different roughness categories, to predict IRI values, and to detect the presence of aggregate segregation on the pavement surface of a newly-constructed road section.

3. LITERATURE REVIEW

3.1 Computer Vision Applications in Transportation

In pavement engineering, computer vision approaches have been successfully used and implemented to extract features in the pavement surface from captured images. Researchers have applied different computer vision approaches to detect and classify distresses such as cracks, potholes, and raveling. Furthermore, researchers have used computer vision applications in estimating the type and extent of detected pavement distresses.

The early efforts in developing crack extraction algorithms were focused in statistical intensity thresholding approaches. Till date, this technique has been used by many researchers due to its simplicity and efficacy. Maser in 1987 proposed a threshold-based segmentation for image analysis by enhancing the image using histogram equalization *(7)*. Li et al. employed a combination of image histogram and projection histogram to separate the non-distress objects such as road markings, oils, and tire marks from major distresses on flexible pavements *(8)*. Koutsopoulos and Downey employed the regression-based histogram method to provide best results compared to other three intensity thresholding methods *(9)*, which included Otsu's method *(10)*, relaxation method, and Kittler's method *(11)*. The authors developed image enhancement, segmentation, and distress classification algorithms to address different distress types in flexible pavements. A different approach was suggested for image binarization, which assigned a value of 0 to 3 to each pixel based on its probability of belonging to the object *(9)*.

Georgopoulos et al. developed an algorithm based on a software known as 'APDIS' to automatically identify the type, extent, and severity of pavement cracking *(12)*. Xu and Huang developed an algorithm based on 'grid cell' analysis, which divides the pavement into small cells and a cell is classified as a crack or non-crack based on the statistical characteristics *(13)*. Wu et al. developed a crack recognition and segmentation algorithm namely MorphLink-C; the algorithm mainly consisted of two processes; (a) using morphological dilation transform to group crack fragments and (b) using thinning transform to connect the fragments *(14)*.

Wavelet transforms, edge detection, and texture analysis are three others widely used techniques in pavement crack detection *(15)*. Zhou et al. used wavelet transform to separate road distresses into high-amplitude wavelet coefficients and pavement noise to low-amplitude wavelet coefficients before applying statistical functions to detect and classify cracks *(16)*. Ying and Salari proposed a beamlet transform based technique in order to extract linear features such as cracks in pavement after application of an image enhancement algorithm *(17)*. A method based on 2D wavelet continuous wavelet transform was applied to detect pavement cracks by Subirats et al. *(18)*. A multiscale complex coefficient maps were created before the application of an algorithm to search wavelet coefficient maximal values and their propagation through the scales for crack detection. However, the wavelet transform techniques has limitation in detecting high curvature or low continuity cracks *(15)*.

In edge detection techniques, algorithms are applied to search and detect edges (defined as sharp intensity transitions) without any inputs or human interference. Abdel-Qader et al. used bidimensional empirical mode decomposition (BEMD) smoothing method to remove noise and applied sobel edge detection technique to detect cracks *(19)*. The sobel edge detection technique was observed to produce better results for images with less irregularities and noise *(20)*. Maode et al. employed morphological operation tools to detect, extract, and fill the crack edges. The

procedure consisted of the application of morphological gradient operator with morphological closing operator after the use of median filter to smooth and enhance pavement image *(21)*. The texture analysis techniques employ crack extraction algorithms to separate cracks from highly textured pavements.

Song et al. presented an algorithm based on Wigner distribution to segment cracks from complex textured background. This model was found highly effective and was more accurate than Fourier based crack detector in terms of locality and discriminatory power *(22)*. In a study by Hu and Zhao, a gray-scale and rotation invariant operator known as local binary pattern (LBP) was used for texture classification and crack detection *(23)*. Despite certain improvements in various image processing techniques, researchers still encounter various challenges in image processing due to texture inhomogeneity of pavement aggregate, random non-crack background noises, spots and stains, oils, road markings and so forth. These challenges demand further advancement in image preprocessing and thresholding techniques to precisely assess flexible pavement conditions.

3.2 Latest Advancements in Image-Based Crack Detection Techniques

3.2.1 Convolution Neural Networks (CNN)

Computer vision approaches based on Deep Learning (DL) techniques have gained significant attention in recent years in pavement engineering particularly for distress detection and classification. The four main DL architectures include Restricted Boltzman Machines (RBMs), Deep Belief Networks (DBNs), Autoencoder (AE), and Deep Convolutional Neural Networks (DCCNs or Deep ConvNets) *(24)*.

CNN are a specialized type of Artificial Neural Networks (ANN) that employs a mathematical operation known as convolution instead of general matrix multiplication. They are well suited for the handling of image-based (pixel) data *(25)*. A deep convolutional neural network is a part of an ANN with one or more convolutional layers, which are mainly used for image processing, classification, and segmentation *(26)*. The feature extraction network analyzes the input image, and the classification neural network operates on the image based on its features. It automatically detects the features on the images using multiple convolutional layers, pooling layers, and fully connected layers. The first two layers focus on extracting features from the image, and the fully connected layer provides features as output. This model is developed using a deep learning method through transfer learning. A detailed overview of the use of CNN in pavement applications has been presented by Dhakal *(27)*.

3.2.2 Use of Deep Learning Techniques in Pavement Applications

In recent years, there has been a significant improvement in crack recognition, classification, and characterization approaches that use computer vision techniques. These techniques are considered as promising approaches to automatically assess pavement conditions in terms of cracking by analyzing the pavement images. Koch et al. in their review reported the increasing use of high-level computer vision techniques such as neural models and support vector machines (SVM) with image processing in segmentation, classification, and feature extraction of pavement cracks *(28)*. Moussa and Hussain used SVM to classify surface cracks as transverse, longitudinal, block, and alligator cracking after the images were segmented using graph cut segmentation procedure *(29)*. Nguyen et al. combined Conditional Texture Anisotropy (CTA) method of crack segmentation

with multi-layer perceptron neural network and classified the detected defect as cracks, joint, and bridged *(30)*.

Mokhtari et al. compared four computer-vision based crack detection systems namely artificial neural network (ANN), k-nearest neighbor, decision tress, and adaptive neuro-fuzzy inference system (ANFIS). ANN and ANFIS methods were observed to be more accurate in terms of performance prediction, computation time, and stability of the results and classifiers' performance *(31)*.

Deep Learning (DL) based computer vision approaches have gained significant acceptance amongst pavement researchers in recent years, particularly for distress classification *(32)*. Deep Convolutional Neural Networks (DCCNs) are typically composed of convolutional, pooling and fully connected layers; a filter bank, which is a set of weights connects units in the feature maps of convolutional layers to local patches in the feature maps of the input data. In addition, the pooling layer units receives the maximum of a local patch of units in one feature map and also reduces the resolution of feature maps to select the spatial invariance, and the fully connected layers are like traditional multi-layer perceptron in which all units in the feature maps are concatenated together into a form of a vector *(33)*.

Zhang et al. developed an automatic crack detection DCNN based on the manually annotated image patches as inputs *(34)*. The dataset consisted of 500 pavement images of size 3264x2448 collected using a smart phone. The collected pavement images were sampled to generate one million three-channel (RGB) 99x99-pixel image patches; 640,000 samples were used for training, 160,000 samples were used for validation, and 200,000 samples were used for training. The developed solution classified the crack and non-crack pixels referred to as positive and negative patches respectively based on a ConvNet trained in square image patches. The training process was amplified using the rectified linear units (ReLU) activation function. Figure 2 illustrates the architecture of proposed DCNN *(34)*.
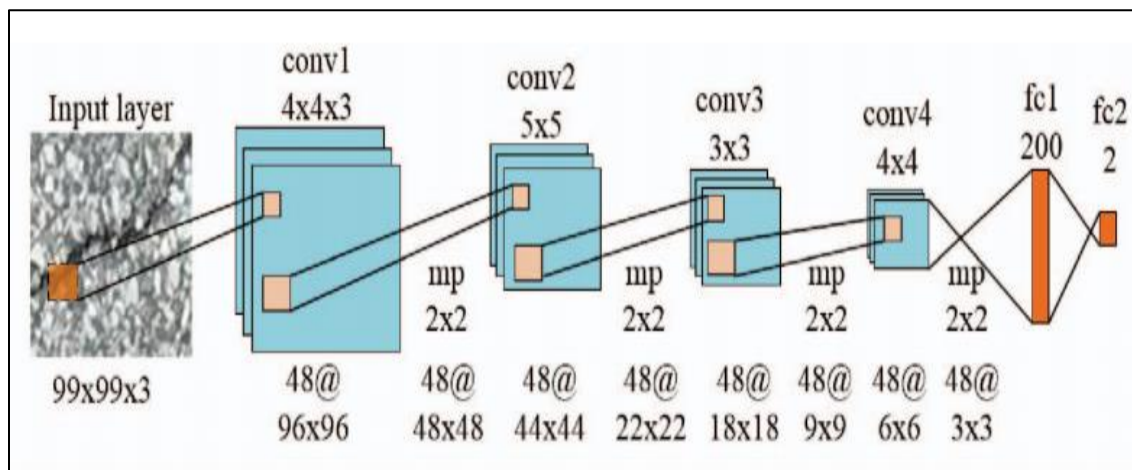

Figure 2. Architecture of Proposed DCNN *(34)*

Elisenbach et al. (2017) developed a convolutional neural network for road crack detection and named it as RCD net, which used the same four-block ConvNet developed by Zhang et al. *(35)*. The German Asphalt Pavement Distress (GAPs) dataset was introduced as an attempt to create a standard benchmarking pavement distress dataset for DL applications *(36)*. A DL approach,

ASINVOS, which consisted of eight convolutional layers, three max-pooling layers, and three fully-connected layers was implemented to study the regularization effects on the generalization ability of DCNN; the proposed approach was observed to outperform the traditional distress detection approaches with higher generalization ability *(36)*.

Fan et al. proposed an automated crack detection procedure based on structural prediction using CNN. The CNN modeled as a multi-label classification problem consisted of four convolutional layers, two max-pooling layers, and there fully-connected layers. The overall pavement condition was presented by probability map obtained by summing the center patch structure predictions of the trained CNN applied on all pixels. The proposed method was observed to be superior compared with other existing methods of crack detection *(37)*. The CNN used by the authors is illustrated in Figure 3. The convolutional layers were with kernel of 3 x 3, stride 1 and zero padding and max pooling was performed with a stride 2 over a 2 x 2 window.
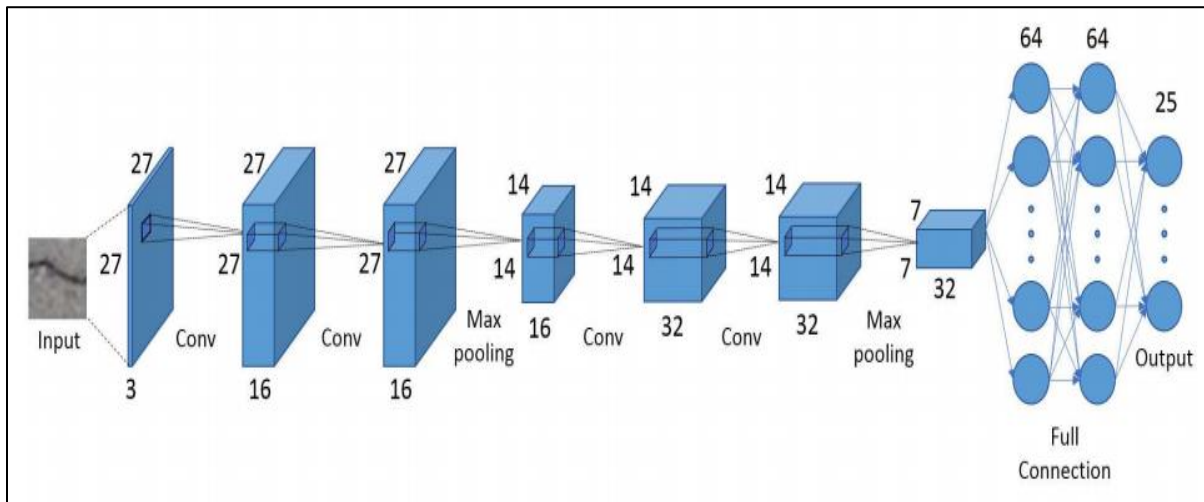

Figure 3. CNN Architecture *(37)*

3.3 Roughness Prediction

Several approaches were developed during the last two decades for the prediction of IRI values from pavement characteristics such as pavement age, structural capacity, traffic volume, and climatic data. Rosa et al. conducted a study to predict the IRI value from the initial IRI value and pavement age based on data collected from the Texas Department of Transportation from 2005 to 2014. The pavement sections were categorized based on climatic conditions, subgrade soil, treatment type, pavement type, traffic loading, and functional level. The regression coefficients were then fitted for each category *(38)*. The proposed regression model was as follows:

$$\ln\left(\frac{IRI_i}{IRI_n - IRI_i}\right) = \beta_3 + \beta_2 e^{Time\beta_1} \tag{1}$$

where,

IRI_i = initial IRI;

IRI_n = IRI in year n;

Time = number of years since IRI_i; and

β_1, β_2, β_3 = calibration parameters.

A nonlinear least-square method was used to determine the calibration coefficients. A comparison between measured versus predicted IRI is presented in Figure 4. The error in prediction was around 20 in./mile, which was deemed reasonable at the network level. In addition, the empirical model was more accurate for low to medium traffic loading with a RMSE of around 7%.
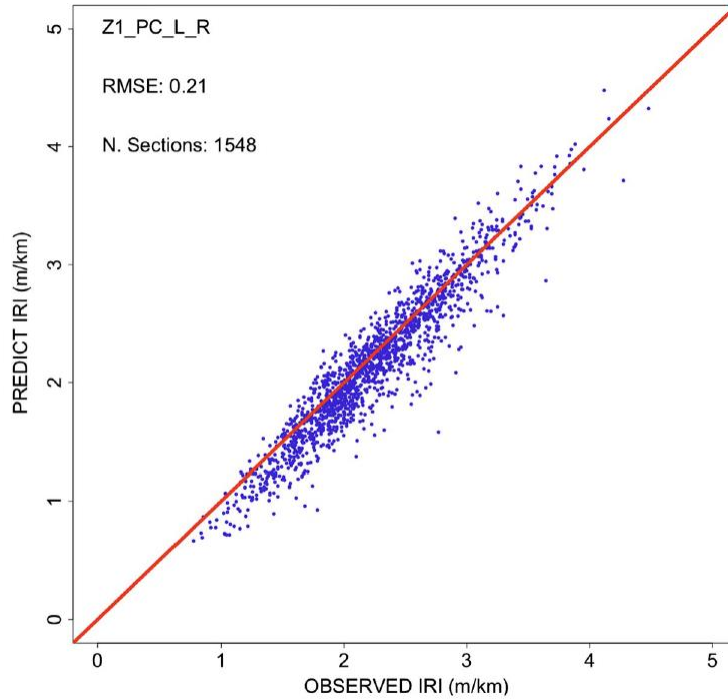

Figure 4. Predicted versus Measured IRI in 2015 *(38)*

Similarly, Khattak et al. developed a model to predict IRI value for Asphalt Concrete (AC) overlay based on climatic and traffic data, age of treatment, functional classification, and pavement thickness *(39)*. Performance data from Louisiana were used to calibrate and validate the models. For flexible pavements, the following regression model was developed:

$$\ln(\text{IRI}) = a_0 + a_1\left(\frac{1}{F_n}\right) + a_2\left(\frac{\ln(CESAL)}{T_0}\right) + a_3.\,T_1 + a_4.\,CPI.\,t + \Delta \quad (2)$$

where,

IRI = International Roughness Index (m/km);

F_n = functional classification;

CESAL = cumulative equivalent single-axle load (ESAL);

T_o = thickness of overlay;

T_1 = temperature index;

5

T = age of treatment;

CPI = cumulative precipitation index;

$\Delta = 4.388 + 0.723 . \ln (SD_o) + 0.513 . \ln (IRI_{pp})$;

SD_o = initial Standard Deviation (SD);

IRI_{pp} = predicted IRI of the previous year.

Figure 5 presents a comparison of the predicted versus measured IRI. As shown in the figure, the model predicted IRI with an overall accuracy of 0.47 as depicted by the coefficient of determination (R^2).
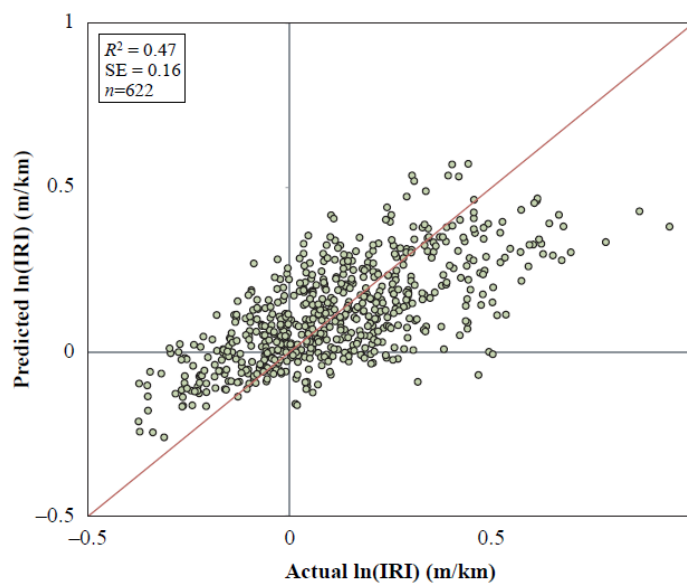

Figure 5. Predicted versus Measured IRI for Flexible Pavement Sections *(39)*

Albuquerque and Nunez analyzed the data collected on 45 low-volume road sections to develop an IRI model for AC and asphalt surface treatments. The IRI value was estimated based on a local climatic index, the modified structural number (SNC), and the cumulative numbers of equivalent single-axle loads *(40)*. Moreover, Qian et al. presented an IRI prediction model for thin overlays based on data collected from 79 Long-Term Pavement Performance (LTPP) road sections. The data were categorized into three groups based on temperature. For each group, an IRI model was developed based on the variables that significantly affected the model's accuracy *(41)*.

Sandra and Sarkar utilized distress data collected on a 40.0-km (24.5-mile) pavement segment in India to develop a model for IRI prediction *(42)*. The authors predicted the IRI value based on pavement surface distresses including cracking, potholes, patching, rutting, and raveling *(42)*. Similarly, Abdelaziz et al. used LTPP data to predict the IRI values from existing pavement surface distresses. Data from 506 sections including initial IRI, age, and pavement surface distresses were used to develop the regression model *(43)*. In Canada, Patrick and

Soliman utilized roughness and distress data from the LTPP to develop IRI prediction models for dry-freeze and wet-freeze regions *(44)*.

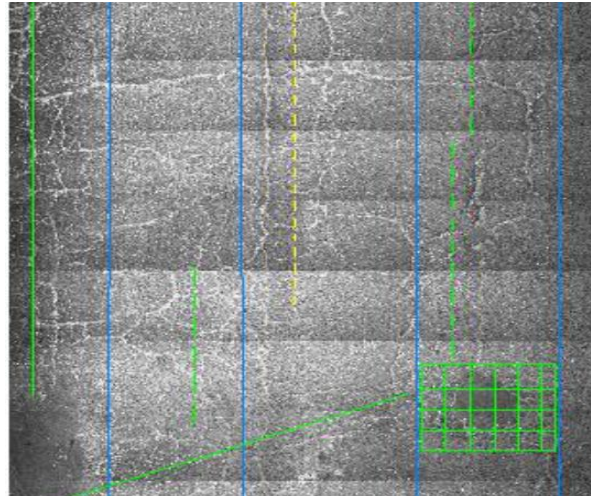### 3.3.1 Machine-Learning Models

In recent years, machine-learning approaches have gained significant interest amongst pavement researchers. Sandra et al. collected distress data on 617 kilometers (383.4 miles) of pavement sections in India to train an ANN model for IRI prediction *(45)*. The data were clustered into eight groups; an ANN model was then developed for each group *(45)*. Abdelaziz et al. proposed a forward back propagation ANN to predict IRI values based on distress data and pavement age *(43)*. Similarly, Ziari et al. developed an ANN model using data obtained from 26 flexible LTPP sections. Pavement age, thickness, climate, and traffic data were the input variables used to predict IRI *(46)*. Hossain et al. proposed an ANN model to predict IRI for flexible pavements based on climatic and traffic data in Illinois *(47)*.
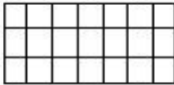
3.4 Louisiana Pavement Management System

The pavement network in Louisiana is surveyed every two years using the Automatic Road Analyzer (ARAN) system, which acquires continuous high definition digital images of the pavement surface *(48)*. This specific vehicle, shown in Figure 6, is equipped with cameras, lasers, sensors and computers to collect high-definition digital images of the pavement surface and right of way and electronic data of pavement distresses namely cracking, rutting, faulting, IRI, and macrotexture for both primary (i.e., South to North or West to East) and secondary (North to South or East to West) directions. While the ARAN is equipped with a GPS unit, the data are collected and reported for every 1/10th of a mile of the road network. The continuous digital images and distress data (VISIDATA) acquired by ARAN are utilized by each district, and the personnel has been trained to use the data. When collecting pavement images, the various types of cracks are identified by distress category, rated in order of severity, measured, and recorded in the database; see Figure 7(a). Symbols indicate distress category and a three-color system is used to distinguish severity levels as shown in Figure 7(b) *(49)*.

Figure 6. The Automatic Road Analyzer (ARAN) system

(a) Image by ARAN

(b) Distress Identification

Figure 7. The Automatic Road Analyzer (ARAN) system *(49)*

The Louisiana Department of Transportation and Development (LaDOTD) also measures and monitors pavement roughness conditions based on the measurements of an inertial profiler (automated profiler). Inertial profilers approximate the actual pavement profile using non-contact sensors to quantify the relative vertical shift between the vehicle frame and the road surface. The collected data are then used to calculate the IRI values using a quarter-car mathematical model (TR 6442017). Pavement sections are categorized and ranked based on the measured IRI values, as depicted in Table 1.

Table 1. IRI Thresholds for Different IRI Categories *(2)*

IRI Rating		IRI Range (in./mile)
1	**Very Good (VG)**	<90
2	**Good (G)**	90-180
3	**Fair (F)**	180-258
4	**Poor (P)**	>258

3.5 Aggregate Segregation

Two types of segregation can affect the quality of asphalt paving construction, namely, aggregate segregation and temperature segregation. Aggregate (gradation) segregation, which is the main type of segregation and is the focus of this study, is caused by the concentration of coarse aggregate in some areas and fine aggregate in others. On the other hand, temperature segregation is defined as a temperature differential exceeding 14°C in the paving mat, which may cause weak spots on asphalt pavements. While the negative effects of aggregate segregation have a long history of thorough investigations in the literature, debate exists on the significance of thermal segregation on pavement performance *(50)*.

Aggregate segregation is a major concern for highway agencies as it can cause a reduction in pavement life by as much as 50% *(51)*. This problem has persisted even after the introduction of the Superpave specification system in the early 1990s and the Material Transfer Vehicle (MTV) in the late 1990s. A segregated asphalt mixture does not conform to the original job mix formula (JMF) in gradation and/or asphalt binder content, creating a difference in the expected density and air void content of the mix as compared to the job mix formula. Research has shown that segregated mixes exhibit reduced service life as compared to unsegregated mixes due to diminished stiffness, tensile strength, and fatigue life *(52)*. Laser profiling and infrared thermography have successfully been used to detect segregation.

3.6 Limitations in the Current State of Practice

From the literature review, it can be concluded that while pavement condition evaluation has gradually transitioned to automated collection and computer vision methods, construction monitoring and acceptance are still mainly based on destructive and slow testing methods. While the use of smoothness specifications is a positive development in pavement engineering to assess construction quality, the unavailability of a profiler in a road construction project is a major obstacle for widespread implementation of this practice. This may result in inadequate construction quality and the inability to introduce timely remedies to address noted deficiencies. While regression and ANN models were developed to predict surface roughness, the following limitations are noted:

- Current models, which were developed based on distress data, exhibited low accuracies in IRI prediction. Abdelaziz et al. obtained coefficients of determination (R^2) values of 0.57 and 0.75 for the regression and ANN models, respectively, when the measured and predicted IRI values were compared *(43)*. Similarly, Patrick and Soliman reported an R^2 of 0.76 and 0.44 for dry freeze and wet freeze regions, respectively *(44)*.
- Available models require a wide number of input variables, which may not be available to the user. For instance, the model developed by Khattak et al. requires ESALs, thickness of overlay, temperature index, age of treatment, precipitation index, and initial IRI *(39)*.
- Numerous models incorporated pavement structural capacity as an input for IRI prediction *(40)*. The use of a pavement structural capacity component in predicting a functional condition index such as IRI is questionable. For example, Albuquerque et al. incorporated the modified structural number (SNC) as an input variable into the IRI prediction model *(40)*.

4. METHODOLOGY

4.1 Roughness Detection

Figure 8 describes the general outline of the research methodology. First, the LaDOTD PMS was used to extract IRI data for newly constructed pavement sections, which were used in the development and validation of the CNN models for roughness and IRI prediction. Afterwards, the I-Vision software was used to extract pavement surface images for these sections at the same locations of the IRI measurements. These images were then categorized into two groups, "VG" and "G" according to Table 1. CNN models were then trained and validated using the extracted PMS data. It is worth noting that the focus of the study was only on newly-constructed roads, which explain the categorization of the images in the very good and good categories.
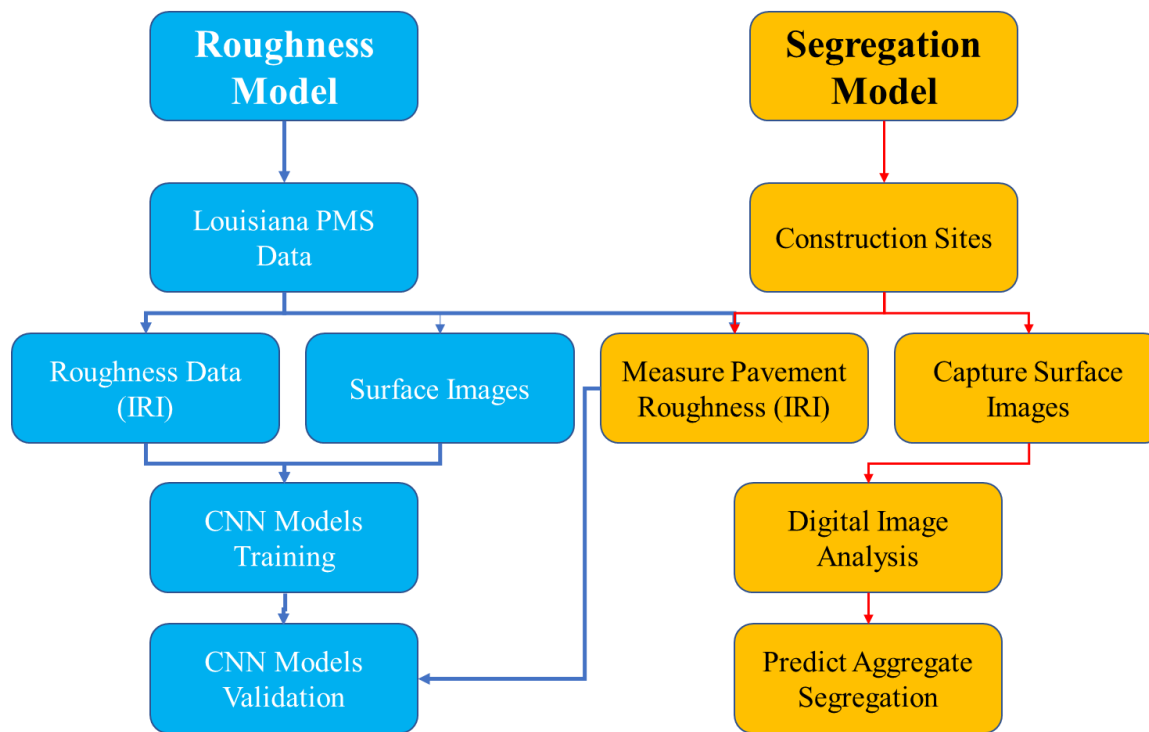

Figure 8. Outline of the Research Methodology

Twenty-two pavement sections, which were surveyed using ARAN within two years of their construction, were selected for development of the IRI model. A total of 600 images were collected from these sections in addition to their corresponding IRI values. Description of these 22 pavement sections is provided in Table 2. As shown in Table 2, the IRI values of the selected pavement sections ranged from 50 in/mi (0.79 m/km) to 180 in/mi (2.84 m/km) after one to two years of construction, covering a wide range of initial roughness values that were needed to train a robust deep learning model.

To assist in the training and validation of the roughness model and the development of the segregation model, three newly-constructed sites were surveyed in the study. For these sites,

pavement surface images were collected using an iPhone 11 smart phone as illustrated in Figure 9. Overall, a total of 129 pictures were collected from these sections. The project contactor measured surface roughness in these pavement sections using a lightweight profiler. Collected data were analyzed using PROVAL software to calculate the IRI values, which ranged from 20.1 in./mile to 74.8 in./mile with an average of 41.0 in./mile.

Table 2. Description of the Pavement Sections Extracted from Louisiana PMS

Section	Pavement Length (mi.)	Date Constructed	Date of survey	Years in Service	Average IRI[1]
1	1.35	2018	2019	2	168
2	2.77	2018	2019	2	146
3	0.99	2018	2019	2	85
4	0.31	2018	2019	2	82
5	10.86	2019	2019	1	73
6	15.48	2018	2019	2	65
7	0.67	2019	2019	1	127
8	6.17	2018	2019	2	68
9	1.82	2019	2019	1	62
10	3.61	2018	2019	2	76
11	1.70	2018	2019	2	58
12	7.37	2018	2019	2	59
13	2.37	2018	2019	2	113
14	7.12	2018	2019	2	64
15	7.27	2018	2019	1	102
16	7.00	2018	2019	2	116
17	5.70	2019	2019	1	156
18	0.40	2018	2019	2	92
19	5.41	2019	2019	1	50
20	1.73	2018	2019	2	53
21	6.08	2018	2019	2	124
22	5.83	2018	2019	2	71

[1] IRI in in./mile.

Figure 9. Illustration of Data Collection Process at the Construction Site

4.2   Detection of Aggregate Segregation

For the development of the segregation model, pavement surface images were collected from the construction sites a few days after construction was complete; see Figure 9. The images were converted into grayscale images, and image thresholding was conducted to assist in separating foreground and background surfaces. Afterwards, the aggregate particles were detected using contour, which also allowed to determine the diameter of each aggregate particle exposed on the pavement surface. The captured surface image was then divided into 64x64 equal squares. A segregation parameter (S) was then defined according to Equation (3) to assess the relative distribution of particle aggregate size on each of the 4,096 squares (64x64). For each of the squares defined in the picture, the aggregate segregation parameter was calculated according to Equation (3):

$$S_i = (\frac{\text{Average diameter of aggregate in any square (i)}}{\text{Average diameter of aggregate in the entire pictiure}} - 1) \ 100\% \qquad (3)$$

It is noted that a S-value of 0% would indicate no segregation while a S-value of 100% would indicate severe (or maximum) segregation.

4.3   Image Processing and Filtering

To enhance the quality of the images and the accuracy of the machine learning models, pavement images obtained from the LaDOTD PMS and construction sites were pre-processed as illustrated in Figure 10. Image processing allowed to enhance the features of the image from the background and noise prior to using them as training, testing, and validation data sets in CNN. The image pre-processing technique involved five major steps namely image acquisition, median filtering, morphological erosion, contrast enhancement, and background subtraction as illustrated in Figure 10.
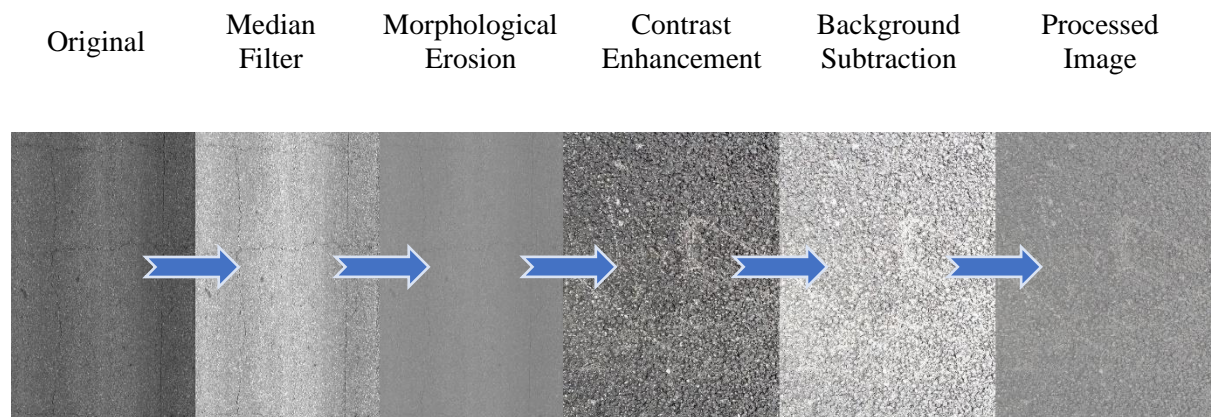
Original	Median Filter	Morphological Erosion	Contrast Enhancement	Background Subtraction	Processed Image

Figure 10. Illustration of Image Processing and Filtering Steps

4.4 CNN Model

In this study, a deep convolutional neural network model was developed to predict the roughness of newly constructed flexible pavement sections. The study developed two CNN models, one model predicted the roughness categories (Good or Very Good) from the feature analysis of the pavement images. The second model predicted the roughness values using IRI from the feature analysis of the pavement images. To develop these models, collected pavement images were randomly divided into 70%, 15%, and 15% for training, validation, and testing, respectively.

To develop the CNN models, the ResNet Architecture was selected. The fitted ResNet architecture consisted of 18 deep layers, including 17 convolutional layers and one fully connected layer; see Figure 11. The main idea of ResNet is the use of jumping connections or identity connections. The connections function by hopping over one or multiple layers forming shortcuts between these layers. The purpose of establishing these shortcut links was to address deep networks' common problem of disappearing gradients. The utilization of earlier layer activations results from the identity mapping's initial inaction beyond skipping connections. By omitting the connection, the network is compressed, which speeds up network learning. The layers are then expanded once the connections have been compressed so that the remaining portion of the network can learn and explore additional feature space *(53)*.
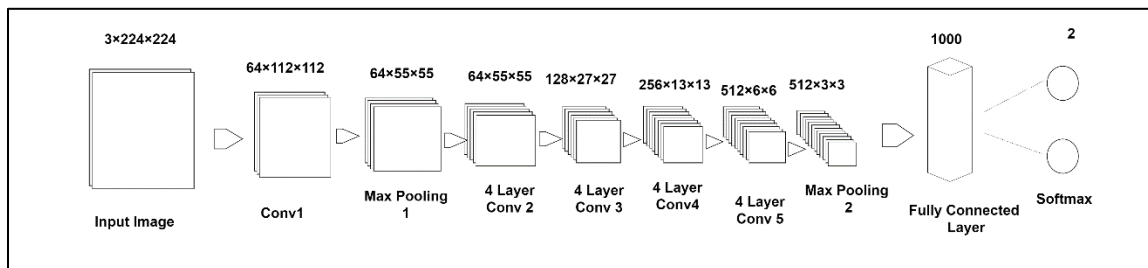

Figure 11. Illustration of the Developed CNN Model Based on the ResNet 18 Architecture

5. RESULTS AND ANALYSIS

5.1 Prediction of Roughness Categories

The accuracy of the CNN model was expressed in the form of confusion matrices, which present the actual and predicted roughness categories (Good or Very Good) in terms of number and percentage. The confusion matrices have two dimensions, one with the actual class of the input and the other with the predicted class, and are used to present the accuracy of the system. Figure 12 illustrates the confusion matrices for the training and validation phases for the IRI categories CNN prediction model. As shown in this figure, the roughness classification model achieved an overall accuracy of 93.8% in the training phase and 92.6% in the validation phase.
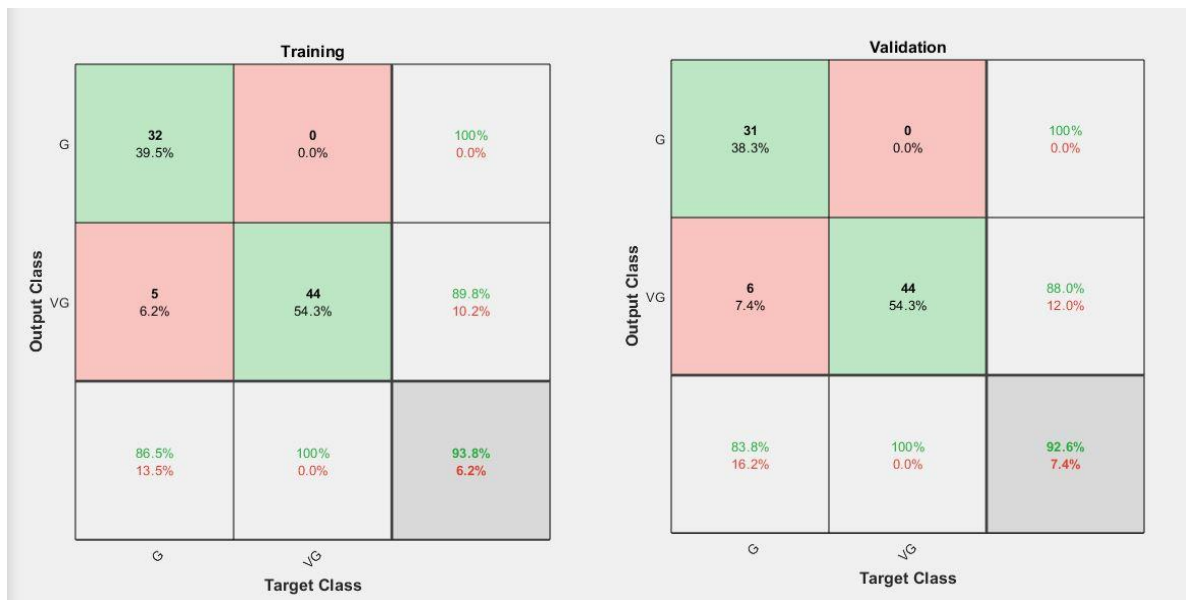

Figure 12. Confusion Matrices for IRI Categories Prediction in (a) the Training and (b) the Validation Phases

5.2 IRI Values Prediction

A second CNN model was developed to predict the IRI values of newly-constructed flexible pavement sections. The model was developed using 600 pavement images collected from the LaDOTD PMS database and 129 pavement images collected from the construction sites. These images were randomly divided into 70%, 15%, and 15% for the training, testing, and validation phases, respectively. The images from the two data sources were used in the three phases to adapt the model to accurately respond to both types of pavement images. Figure 13(a) illustrates the relation between the measured and predicted IRI values. As shown in this figure, the CNN model predicted the IRI value with a coefficient of determination (R^2) of 0.99 and a root-mean-square error (RMSE) of 3.5%, which was acceptable. With respect to precision, Figure 13(a) illustrates a slope and intercept of 0.9879 and 0.0019 m/km of the unconstrained regression line between the measured and predicted values indicating no bias in the model prediction. Furthermore, Figure 13(b) indicates that the mean absolute error was 3.5% indicating acceptable prediction of the IRI values.
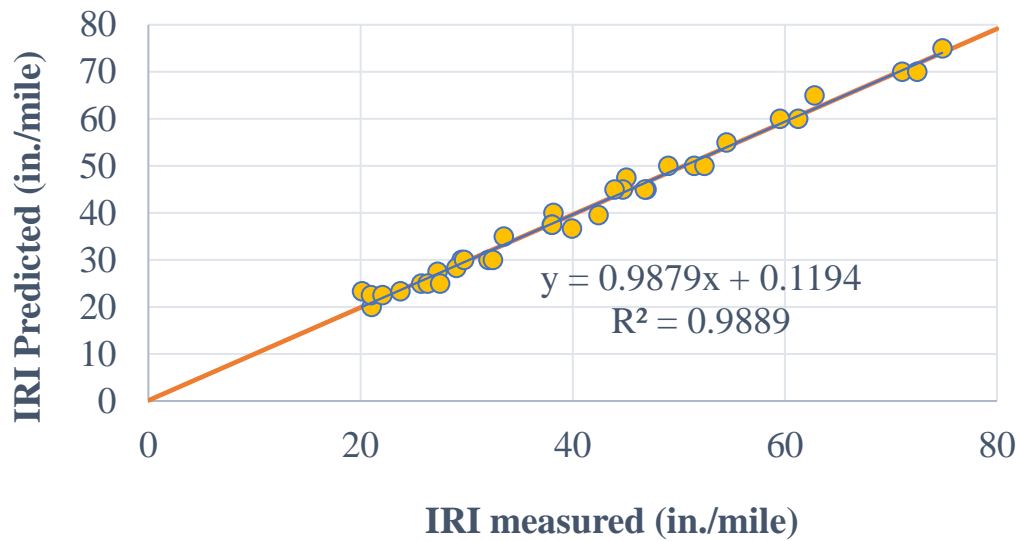
(a)
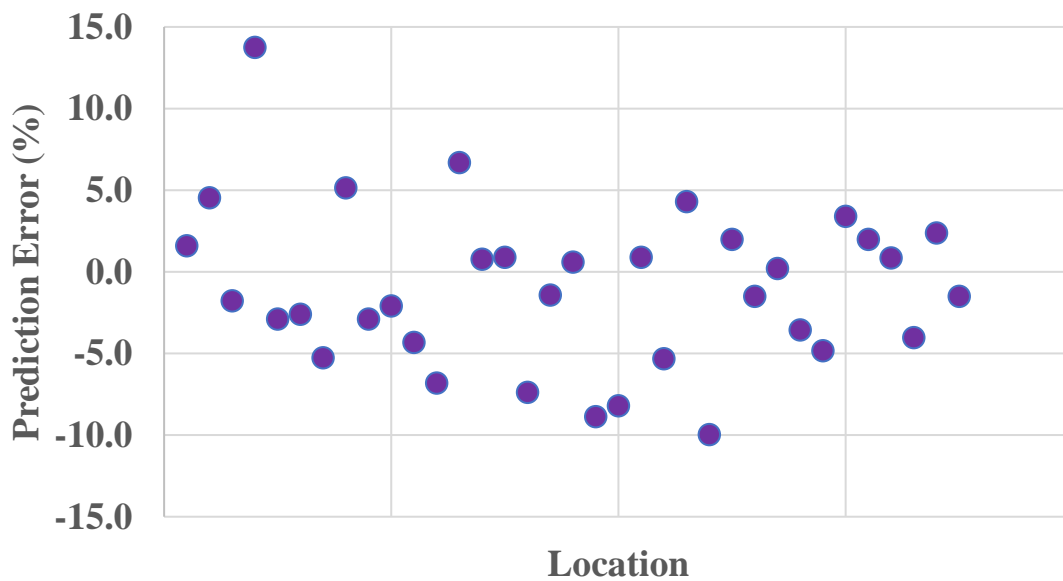
(b)

Figure 13. (a) Relation between the measured and predicted IRI values and (b) Residual errors in the CNN predicted IRI values

5.3 Detection of Segregation

Aggregate segregation on the pavement surface was predicted using digital image analysis as presented in Equation (3). The S-value determined from Equation (3) was used to detect and quantify the presence of segregation on the pavement surface. A S-value of zero indicates no aggregate segregation, a positive value indicates a coarse aggregate segregation, while a negative value indicates a fine aggregate segregation. By categorizing the S-value for each square on the captured image, a colored map was generated based on the calculated S-values for the 4,096

15

squares on the image. A green color, which has a S-value between 0 and 25%, implies very low segregation. A yellow color, which has a S-value between 25 and 50%, implies low segregation. An orange color, which has a S-value between 50 and 75%, implies moderate segregation. Finally, a red color, which has a S-value between 75 and 100%, indicates severe segregation. Figure 14 illustrates two contrasting locations on the pavement surface. Figure 14(a) had significant coarse segregation while Figure 14(b) had low segregation levels on most of the locations. Visual comparison between the digital images and the colored segregation maps presented in Figure 14 showed good visual agreement.
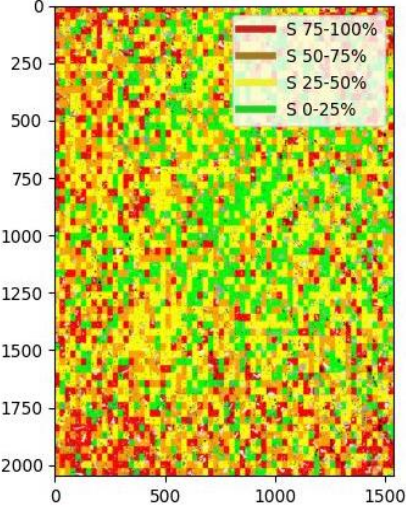
(a)
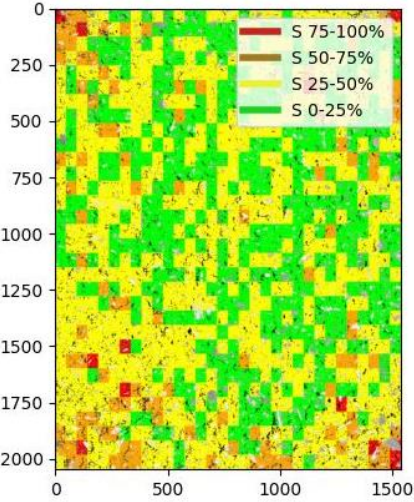
(b)

Figure 14. Pavement surface images and their corresponding S-Plots for (a) a Severely Segregated Location and (b) a Low Segregated Location

5.3.1 Relation between Mix Density and Aggregate Segregation

Research studies have shown good correlation between aggregate segregation and mix density as moderate to severe segregation leads to an increase in air voids and to a decrease in mix density *(52)*. To this end, the relation between the measured mix density using a non-nuclear asphalt density gauge, and the predicted segregation based on the S-values was investigated for more than 25 locations and is presented in Figure 15. As shown in this figure, there was a good correlation between the S-value and the measured mix density with a coefficient of determination (R^2) of 0.92. As the measured mix density decreased, the S-value at this location increased indicating the detection of segregation.
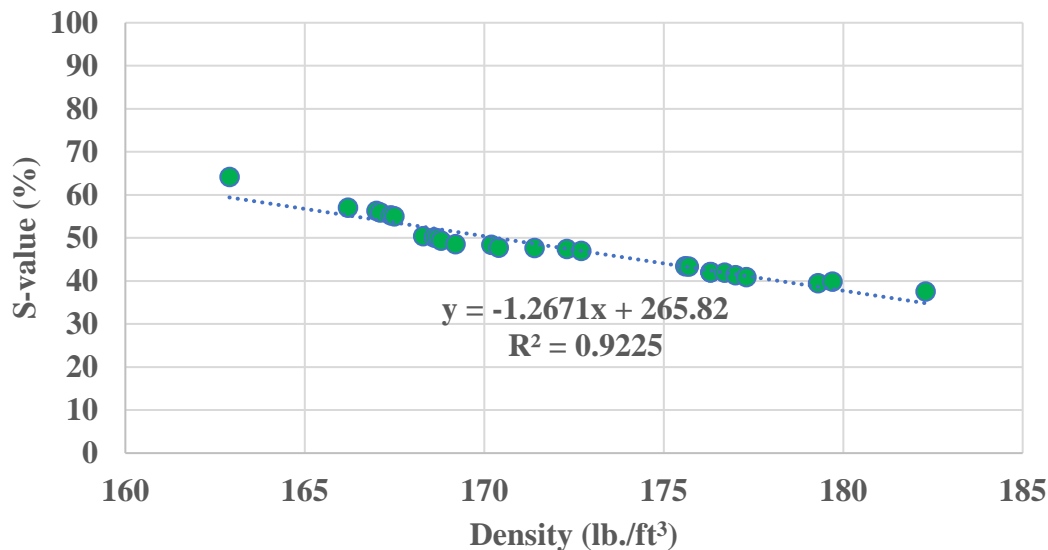

The fitted relation is:

$$y = -1.2671x + 265.82$$
$$R^2 = 0.9225$$

Figure 15. Relation between Mix Density and Segregation Parameter (S-Value)

5.4 Development of a Computer Application

This study developed a Windows-based software application that may be used to predict the roughness categories and IRI values based on the fitted and validated CNN models, see Figure 16. MATLAB-provides an app-design environment known as MATLAB App Designer, which allows to build the user interface and to develop stand-alone Windows-based and MATLAB-based applications. After development, the MATLAB compiler generates an installation file, which can be used to install the application without the need for MATLAB on the user's PC. To use the Windows-based application, the following steps are conducted:

Step 1: Upload the image. The Upload Image button allows the user to browse and open the digital pavement image on their PC for image processing.

Step 2: Image processing. Once the user uploads the image, the application will process the raw pavement image as previously illustrated in Figure 10. This step is conducted automatically without any action from the user.

Step 3: Results. The results of the CNN prediction are predicted at the bottom of the windows. Two results are presented, which are the roughness categories (Good or Very Good) and the predicted IRI values for the conditions pertinent to the uploaded image.
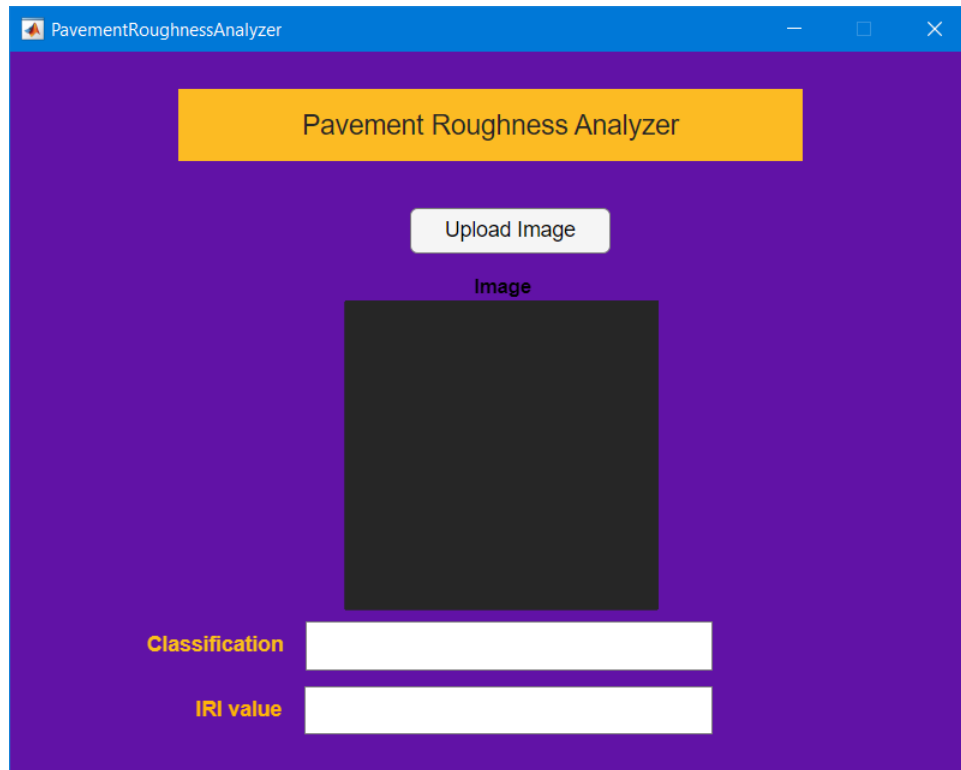

Figure 16. CNN application for the prediction of Roughness Categories and IRI value

Figure 17 illustrates an example of the execution of the Windows-based computer application. The Pavement Roughness Classification and IRI Prediction CNN Model are directly incorporated into the Upload Image push button in the interface. With just one click, the user is able to browse and select the target image, and after a few seconds, the program shows the results for roughness classification and IRI value. The roughness categories are displayed in terms of Good (G) and Very Good (VG), whereas the IRI value can range from 0 to above.
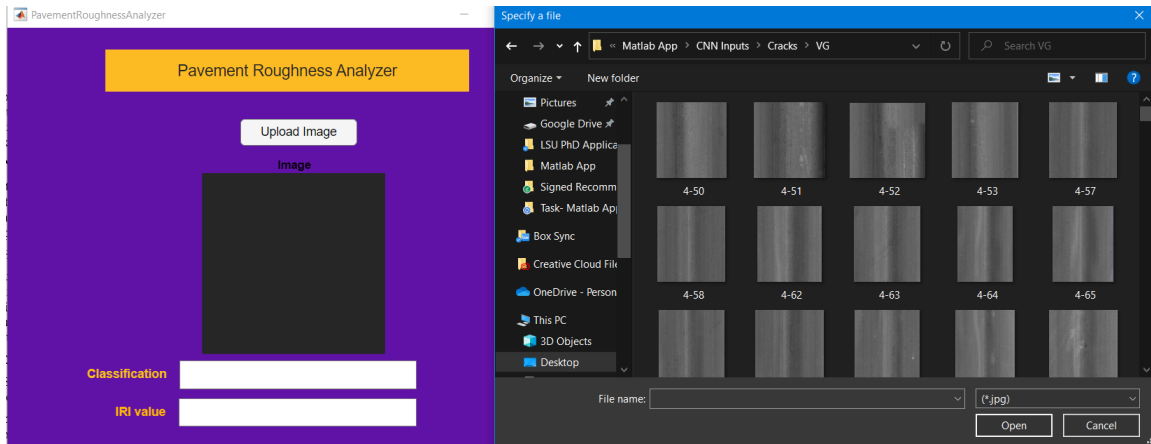
(a)
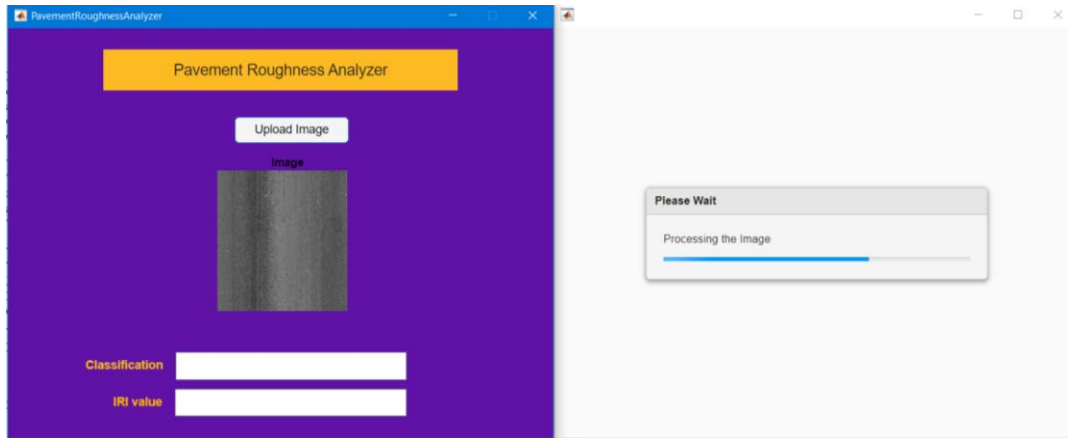
(b)

(c)

Figure 17. Illustration of the Execution of the Windows-Based Computer Application (a) Upload Pavement Image, (b) Processing Image, and (c) Outputs

6. SUMMARY AND CONCLUSIONS

The objective of this study was to develop and validate machine learning models based on Convolutional Neural Networks (CNN) and digital image analysis that can be used to classify pavement surface into different IRI categories, to predict IRI values, and to detect the presence of aggregate segregation on the pavement surface of a newly-constructed road section. To achieve this objective, two CNN models were developed based on the ResNet Architecture. The first model predicted the roughness categories (Good or Very Good) from the feature analysis of the pavement images. The second model predicted the roughness values using IRI from the feature analysis of the pavement images. These models were trained, tested, and validated using 600-pavement surface images extracted from the LaDOTD pavement management system and 129 pavement images collected from three construction sites. These images were randomly divided into 70%, 15%, and 15% for the training, testing, and validation phases, respectively. The images from the two data sources were used in the three phases to adapt the model to accurately respond to both types of pavement images.

For the development of the segregation model, a segregation parameter (S) was introduced to assess the relative distribution of particle aggregate sizes on a grid defined by 4,096 equally-distributed squares. The calculated S-value was then used to detect and quantify the presence of segregation on the pavement surface. A S-value of zero indicates no aggregate segregation, a positive value indicates a coarse aggregate segregation, while a negative value indicates a fine aggregate segregation. By categorizing the S-value for each square on a captured image, a colored map was generated based on the calculated S-values for the 4,096 squares. Based on the results of the analysis, the following conclusions were drawn:

- The roughness classification model achieved an overall accuracy of 93.8% in the training phase and 92.6% in the validation phase.
- The IRI prediction model had an acceptable accuracy with a coefficient of determination (R^2) of 0.99 and a root-mean-square error (RMSE) of 3.5%.
- Visual comparison between the digital images and the colored segregation maps showed good agreement.
- The developed segregation detection procedure adequately described the relationship between mix density and segregation by predicting an increase in S-value with the decrease in mix density.

Based on the results of this study, a computer application was developed for the AI models by creating a standalone tool, which would allow the site engineers to use the developed models without the need for coding software on their device. Future development of the application may allow the users to retrain the adaptive models to ensure up-to-date accuracy.

7. REFERENCES

1. Von Quintus, Harold L. NDT technology for quality assurance of HMA pavement construction. Vol. 626. Transportation Research Board, 2009.
2. Abohamer, H., M.A. Elseifi, N. Dhakal, and Z. Zhang. Development of a Deep Convolutional Neural Network for the Prediction of Pavement Roughness from 3D Images. ASCE, Journal of Transportation Engineering, Part B: Pavements, 147(4): https://doi.org/10.1061/JPEODX.0000310, 2021.
3. Stroup-Gardiner, M. (2015). Methods and Practices on Reduction and Elimination of Asphalt Mix Segregation. NCHRP Synthesis 477, Washington, D.C.
4. ASTM. (2008). Roads and Parking Lots Pavement Condition Index. D 6433 – 07, West Conshohocken, PA 19428-2959, United States: ASTM International.
5. Zhang, A., Wang, K.C.P., Li, B., Yang, E., Dai, X., Peng, Y., Fei, Y., Liu, Y., Li, J. Q., and Chen, C. Automated Pixel-Level Pavement Crack Detection on 3D Asphalt Surfaces Using a Deep-Learning Network. Computer-Aided Civil and Infrastructure Engineering 32: 805-819. DOI: 10.1111/mice.12297, 2017.
6. Wu, H., Yao, L., Xu, Z., Li, Y., Ao, X., Chen, Q., and Li, Z. Road pothole extraction and safety evaluation by integration of point cloud and images derived from mobile mapping sensors. Advanced Engineering Informatics 42. DOI: 10.1016/j.aei.2019.100936, 2019.
7. Maser, K.R. Computational techniques for automating visual inspection. Massachusetts Institute of Technology, Report, Cambridge, MA, 1987.
8. Li, L., Chan, P., Rao, A., and Lytton, R.L. Flexible pavement distress evaluation using image analysis. In Applications of Advanced Technologies in Transportation Engineering, ASCE, pp. 473-477, 1991.
9. Koutsopoulos, H.N., and Downey, A.B. Primitive-based classification of pavement cracking images. Journal of Transportation Engineering, 119, no. 3, pp. 402-418, 1993.
10. Otsu, N. A threshold selection method from gray-level histograms. IEEE transactions on systems, man, and cybernetics, 9(1), 62-66, 1979.
11. Kittler, J., and Illingworth, J. Minimum error thresholding. Pattern recognition, 19(1), 41-47, 1986.
12. Georgopoulos, A., Loizos, A., and Flouda, A. Digital image processing as a tool for pavement distress evaluation. ISPRS Journal of Photogrammetry and Remote Sensing, 50(1), pp. 23-33, 1995.
13. Xu, B., Huang, Y.R. Development of an automatic pavement surface distress inspection system. Report No. FHWA/TX-05/7-4975-1, 2003.
14. Wu, L., Mokhtari, S., Nazef, A., Nam, B., and Yun, H.B. Improvement of crack-detection accuracy using a novel crack defragmentation technique in image-based road assessment. Journal of Computing in Civil Engineering, 30(1), 04014118, 2014.
15. Zou, Q., Cao, Y., Li, Q., Mao, Q., and Wang, S. CrackTree: Automatic crack detection from pavement images. Pattern Recognition Letters, 33(3), 227-238, 2012.
16. Zhou, J., Huang, P. S., and Chiang, F. P. Wavelet-based pavement distress detection and evaluation. Optical Engineering, 45(2), 027007, 2006.
17. Ying, L., and Salari, E. Beamlet transform based technique for pavement image processing and classification. In Electro/Information Technology, 2009. eit'09. IEEE International Conference on, pp. 141-145, IEEE, 2009.

18. Subirats, P., Dumoulin, J., Legeay, V., and Barba, D. Automation of pavement surface crack detection using the continuous wavelet transform. In 2006 International Conference on Image Processing (pp. 3037-3040). IEEE, 2006.
19. Abdel-Qader, I., Abudayyeh, O., and Kelly, M. E. Analysis of edge-detection techniques for crack identification in bridges. Journal of Computing in Civil Engineering, 17(4), 255-263, 2003.
20. Ayenu-Prah, A., and Attoh-Okine, N. Evaluating pavement cracks with bidimensional empirical mode decomposition. EURASIP Journal on Advances in Signal Processing, 2008(1), 861701, 2008.
21. Maode, Y., Shaobo, B., Kun, X., and Yuyao, H. Pavement crack detection and analysis for high-grade highway. In 2007 8th International Conference on Electronic Measurement and Instruments (pp. 4-548). IEEE, 2007.
22. Song, K. Y., Petrou, M., and Kittler, J. Texture crack detection. Machine Vision and Applications, 8(1), 63-75, 1995.
23. Hu, Y., and Zhao, C. X. A novel LBP based methods for pavement crack detection. Journal of pattern Recognition research, 5(1), 140-147, 2010.
24. Gopalakrishnan, Kasthurirangan, Siddhartha K. Khaitan, Alok Choudhary, and Ankit Agrawal. Deep Convolutional Neural Networks with transfer learning for computer vision-based data-driven pavement distress detection. Construction and Building Materials 157: 322-330, 2017.
25. Li, B., Wang, K. C., Zhang, A., Yang, E., and Wang, G. Automatic classification of pavement crack using deep convolutional neural network. International Journal of Pavement Engineering, 1-7, 2018.
26. Zhang, A., Wang, K.C.P., Li, B., Yang, E., Dai, X., Peng, Y., Fei, Y., Liu, Y., Li, J. Q., and Chen, C. Automated Pixel-Level Pavement Crack Detection on 3D Asphalt Surfaces Using a Deep-Learning Network. Computer-Aided Civil and Infrastructure Engineering 32: 805-819. DOI: 10.1111/mice.12297, 2017.
27. Dhakal, N. (2021). Identification of Top-down, Bottom-up, and Cement-Treated Reflective Cracks Using Convolutional Neural Network and Artificial Neural Network (Doctoral Dissertation, Louisiana State University).
28. Koch, C., and Brilakis, I. Pothole detection in asphalt pavement images. Advanced Engineering Informatics 507-517. DOI: 10.1016/j.aei.2011.01.002, 2011.
29. Moussa, G., and Hussain, K. A new technique for automatic detection and parameters estimation of pavement crack. In 4th International Multi-Conference on Engineering Technology Innovation, IMETI, 2011.
30. Nguyen, T. S., Avila, M., and Begot, S. Automatic detection and classification of defect on road pavement using anisotropy measure. In 2009 17th European Signal Processing Conference (pp. 617-621). IEEE, 2009.
31. Mokhtari, S., Wu, L., and Yun, H. B. Comparison of supervised classification techniques for vision-based pavement crack detection. Transportation Research Record, 2595(1), 119-127, 2016.
32. Gopalakrishnan, Kasthurirangan, Siddhartha K. Khaitan, Alok Choudhary, and Ankit Agrawal. "Deep Convolutional Neural Networks with transfer learning for computer vision-based data-driven pavement distress detection." Construction and Building Materials 157: 322-330, 2017.

33. Li, B., Wang, K. C., Zhang, A., Yang, E., and Wang, G. Automatic classification of pavement crack using deep convolutional neural network. International Journal of Pavement Engineering, 1-7, 2018.

34. Zhang, Lei, Fan Yang, Yimin Daniel Zhang, and Ying Julie Zhu. "Road crack detection using deep convolutional neural network." In 2016 IEEE international conference on image processing (ICIP), pp. 3708-3712. IEEE, 2016.

35. Eisenbach, M., Stricker, R., Seichter, D., Amende, K., Debes, K., Sesselmann, M., and Gross, H. M. How to get pavement distress detection ready for deep learning? A systematic approach. In 2017 international joint conference on neural networks (IJCNN) (pp. 2039-2047). IEEE, 2017.

36. Gopalakrishnan, Kasthurirangan. "Deep Learning in data-driven pavement image analysis and automated distress detection: A review." Data 3, no. 3: 28, 2018.

37. Fan, Z., Wu, Y., Lu, J., and Li, W. Automatic pavement crack detection based on structured prediction with the convolutional neural network. arXiv preprint arXiv:1802.02208, 2018.

38. Rosa, F. D., Liu, L., and Gharaibeh, N. G. (2017). "IRI Prediction Model for Use in Network-Level Pavement Management Systems." American Society of Civil Engineers 143 (1). Doi: 10.1061/ JPEODX.0000003.

39. Khattak, M. J., Nur, M. A., Bhuyan, M.R., and Gaspard, K. (2014). "International roughness index models for HMA overlay treatment of flexible and composite." International Journal of Pavement Engineering 15 (4): 334-344. DOI: 10.1080/10298436.2013.842237.

40. Albuquerque, F. S., and Núñez, W. P., (2011). "Development of Roughness Prediction Models for Low-Volume Road Networks." Transportation Research Record. DOI: 10.3141/2205-25.

41. Qian, J., Jin, C., Zhang, J., Ling, J., and Sun, C. (2018). "International Roughness Index Prediction Model for Thin Hot Mix Asphalt Overlay Treatment of Flexible Pavements." Transportation Research Record 2672 (40): 7-13. DOI: 10.1177/0361198118768522.

42. Sandra, A. K., and Sarkar, A. K. (2012). "Development of a model for estimating International Roughness Index from pavement distresses." International Journal of Pavement Engineering 1-10. DOI: 10.1080/10298436.2012.703322.

43. Abdelaziz, N., Abd El-Hakim, R. T., El-Badawy, S. M., and Afify, H. A. (2018). "International Roughness Index prediction model for flexible pavements." International Journal of Pavement Engineering. doi: DOI: 10.1080/10298436.2018.1441414.

44. Patrick, G., and Soliman, H. (2019). "Roughness Prediction Models using Pavement Surface Distresses in Different Canadian Climatic Regions." Canadian Journal of Civil Engineering 46 (10): 934-940. DOI:10.1139/cjce-2018-0697.

45. Sandra, A. K., Vinayaka Rao. V.R, and Sarkar, A. K. (2013). "Road roughness modelling with clustered data using ANN approach." International Journal of Civil and Structural Engineering 4 (1): 20-35.

46. Ziari, H., Sobhani, J., Ayoubinejad, J., and Hartmann, T. (2015). "Prediction of IRI in short and long terms for flexible pavements: ANN and GMDH methods." International Journal of Pavement Engineering 17 (9): 776-788. DOI: 10.1080/10298436.2015.1019498.

47. Hossain, M. I., Gopisetti, L. S. P., and Miah, M. S., (2017). "Prediction of International Roughness Index of Flexible Pavements from." 256-267. DOI: 10.1061/9780784480922.023.

48. Khattak, M.J., Baladi, G.Y., Zhang, Z., and Ismail, S. "A review of the pavement management system of the state of Louisiana-phase," Transportation Research Record: Journal of the Transportation Research Board, 2008, pp. 18-27.

49. Elseifi, M.A., and O. Elbagalati. (2017). Assessment of Continuous Deflection Measurement Devices in Louisiana – Rolling Wheel Deflectometer. Research Report FHWA/LA. 14/581, Louisiana Transportation Research Center, Baton Rouge, LA.

50. Kim, M., P. Phaltane, L.N. Mohammad, and M.A. Elseifi. Temperature Segregation and Its Impact on the Quality and Performance of Asphalt Pavements. Frontiers of Structural and Civil Engineering, https://doi.org/10.1007/s11709-017-0451-5, 2018.

51. Bode, T.A. An Analysis of the Impacts of Temperature Segregation on Hot-Mix Asphalt. Master Thesis, University of Nebraska, Lincoln, Nebraska, 2012.

52. Stroup-Gardiner, M., and Brown, E. R., Segregation of Hot-Mix Asphalt Pavements, NCHRP Report 441, National Research Council. Washington, D. C., 2000.

53. He, K., X. Zhang, S. Ren, and J. Sun, Deep Residual Learning for Image Recognition. In 2016 IEEE Conference on Computer Vision and Pattern Recognition (CVPR), Las Vegas, NV, USA, doi: 10.1109/CVPR.2016.90, pp. 770-778, 2016.